Available online at www.sciencedirect.com
ScienceDirect
Earth and Planetary Science Letters 257 (2007) 391–406
EPSL
www.elsevier.com/locate/epsl

The role of lithospheric gabbros on the composition of Galapagos lavas

A.E. Saal [a,*], M.D. Kurz [b], S.R. Hart [c], J.S. Blusztajn [c], J. Blichert-Toft [d], Y. Liang [a], D.J. Geist [e]

[a] *Department of Geological Sciences, Brown University Providence, Rhode Island 02912, United States*
[b] *Department of Marine Chemistry and Geochemistry, Woods Hole Oceanographic Institution, Woods Hole, Massachusetts 02543, United States*
[c] *Department of Geology and Geophysics, Woods Hole Oceanographic Institution, Woods Hole, Massachusetts 02543, United States*
[d] *Ecole Normale Supérieure de Lyon, CNRS UMR 5570, 69364 Lyon, France*
[e] *Department of Geological Sciences, University of Idaho, Moscow, Idaho 83844, United States*

Received 20 November 2005; received in revised form 24 February 2007; accepted 27 February 2007
Available online 6 March 2007
Editor: R.W. Carlson

Abstract

New geochemical data combined with a compilation of all published data for the Galapagos basalts indicate that the Galapagos Archipelago can be divided into two very different volcanic areas, east and west of the 91° W fracture zone. In both regions, the interaction between plume melts and depleted upper mantle lavas most likely controls the composition of the erupted basalts. However, we find important differences in the trace element compositions between lavas from the two regions. First, Ti/Gd and Nb/La ratios correlate with $^{3}He/^{4}He$, and all three ratios decrease with increasing distance from Fernandina. These correlations suggest that the high Ti/Gd and Nb/La ratios are typical of the plume mantle source that carries the high $^{3}He/^{4}He$ signature. Second, there is an increase in the Ba/Th, K/La, Sr/Nd, Eu/Eu*, Pb/Nd ratios, and a higher $^{87}Sr/^{86}Sr$ at similar $^{143}Nd/^{144}Nd$ (high ΔSr) from west to east across the fracture zone, and from north to south within the eastern region. These geochemical characteristics resemble those of plagioclase-rich cumulates from the oceanic crust and ophiolite complexes. The compositions of the lavas from the eastern region can be explained by interaction of basalts with plagioclase-rich cumulate during melt percolation through the oceanic lithosphere. We argue that kinetic interaction of magmas with plagioclase-rich cumulates, previously formed either in the Galapagos Spreading Center or beneath the leading edge of the plume on the western region, are responsible for the observed composition of basalts erupted in the eastern region.

Keywords: Galapagos; basalt; geochemistry; gabbro

1. Introduction

The geochemistry of oceanic basalts has been a powerful tool in unraveling the composition, the scale of heterogeneity, and the dynamics of the mantle in areas complicated by the juxtaposition of mid-ocean ridges and hot spot magmatism. One of the best known

* Corresponding author. Tel.: +1 401 863 7238; fax: +1 401 863 2058.
E-mail address: asaal@brown.edu (A.E. Saal).

0012-821X/$ - see front matter © 2007 Elsevier B.V. All rights reserved.
doi:10.1016/j.epsl.2007.02.040

examples of hot spot–ridge interaction is the Galapagos Archipelago, whose location adjacent to the Galapagos Spreading Center (GSC) prompted numerous petrological–geochemical [1–8] geophysical [7–14], and fluid dynamics [15–18] studies on the archipelago and the spreading center.

The compositional variation of lavas from the Galapagos Islands partly reflects the mantle heterogeneity beneath the archipelago. Previous studies have invoked the existence of four main mantle components contributing to the magmatism of the islands: two different types of enriched mantle represented by basalts from Pinta and Floreana Islands, a high-$^3He/^4He$ (22 to 29 Ra; [19]) source corresponding to lavas from Fernandina, and a depleted mantle component exemplified by basalts from Genovesa Island [[1,5,8] and references therein]. Although the origin of the enriched and high-$^3He/^4He$ mantle components has been discussed extensively, the role of the depleted component in the Galapagos lavas has received comparatively less attention; it has been interpreted to reflect either the entrained upper mantle [1,5,8] or an intrinsic part of the plume itself [4]. Meanwhile, the impact of the oceanic lithosphere on the geochemistry of the Galapagos basalts has mostly been ignored.

The present study focuses on the depleted mantle component observed in the central region of the Galapagos Archipelago, and the effect that the oceanic lithosphere exerts on the erupted lavas. Although the basalts from the central region of the archipelago most probably represent entrained asthenospheric mantle into the plume, our results indicate that these lavas have unusual trace element signatures compared to normal MORB and suggest the interaction between the lavas and plagioclase-rich cumulates during melt migration through the oceanic lithosphere.

2. Geodynamic background

The Galapagos Archipelago is located in the eastern equatorial Pacific, 1000 km west of South America, and approximately 150 km south of the active Galapagos Spreading Center (GSC). The Galapagos Islands constitute one of the most active volcanic regions in the world with 21 emergent volcanoes, of which 16 have had historic to Holocene eruptions within an area of 45,000 km^2 [1,8]. The islands and numerous seamounts are constructed mainly upon a shallow submarine volcanic platform overlying a young lithosphere <15 Ma old [5,7,9,20].

The Galapagos Islands have been interpreted as the surface manifestation of a mantle plume. Seismic tomography images showing a slow velocity anomaly extending into the lower mantle [11,14] and an anomalously thin mantle transition zone [12] beneath the Archipelago support a hot spot origin for the plume. However, geological, geophysical and geochemical studies have found it challenging to fit all aspects of the Galapagos Archipelago to a "standard" plume model [5]. In contrast to Hawaii, the "archetype" of the plume model, the Galapagos Islands do not form a linear chain; the volcanism is not strictly time-transgressive in the direction of plate motion, nor is there a consistent petrological or geochemical evolution of the volcanism such as seems to be the case for Hawaii. Nevertheless, the ages of the oldest lavas dated from each volcano form an overall progression from young in the west to old in the east [1,2,21]. The islands, as they drift away from the hot spot, have had intermittent eruptions for approximately 3 Ma, as for example in the case of San Cristobal Island [1,2,7,21]. The continuous volcanism in this most easterly island indicates either an extended zone of melting downstream from the plume, or the existence of post-shield extensional volcanism across the Galapagos platform.

The analysis of bathymetric and gravity data by Feighner and Richards [9] indicates that the crustal thickness in the Archipelago increases from approximately 10 km at the margin of the Galapagos platform to as much as 18 km beneath the southeastern end of Isabela Island. Furthermore, their study reveals that the Galapagos platform is built on two lithospheric sectors, west and east of the 91° W fracture zone, which represents an estimated $\sim$3 Ma age discontinuity across the lithospheric boundary. The eastern sector of the Archipelago is underlain by a weak lithosphere with an elastic thickness of 6 km or less, and close to Airy compensation. In contrast, the western sector is flexurally supported by a lithosphere with an elastic thickness of 12 km. Surface wave tomographic study of the upper mantle beneath the Galapagos Archipelago confirms the different thickness of a "high-velocity lid" across the 91° W fracture zone reaching depths of $\sim$70 km beneath Fernandina, and $\sim$40 km beneath the eastern region [14]. Although Feighner and Richards [9] suggest that the age offset across the 91° W fracture zone extends south of the Galapagos Islands, a compilation of magnetic data [20,22] suggests that the age offset terminates within the Archipelago.

The present-day volcanic and seismic activities are also distinctive in both areas of the Archipelago, west and east of the 91° W fracture zone. In the western part of the Archipelago (Fernandina and Isabela Islands) the eruptive edifices are large central shield volcanoes of unusual shape ("inverted soup-bowl") with well-developed calderas. These volcanoes have the most frequent historic volcanic and seismic activity due to their location close to what is considered the leading

(western) edge of the plume with respect to plate motion at Fernandina, the most active volcano in the Archipelago [2,23]. In contrast, the volcanoes in the eastern, central and southern areas (hereafter referred to as the "eastern sector") are seismically less active and present more varied morphologies and eruptive histories. Thicker lithosphere and the present-day higher magma supply rate in the western sector probably are responsible for yielding large volcanic structures [3].

The composition of the Galapagos lavas also varies within the Archipelago, consistent with the differences in volcanic activity. Lavas erupted from the large western volcanoes are moderately fractionated tholeiites that cooled and fractionated at low pressure (1–3 kb) in the crust. In contrast, lavas erupted from small cones and vents in the eastern sector are compositionally diverse, ranging from picrites to basanitoids; they cooled and fractionated below the Moho at pressures >5 kbar [[3] and references therein]. Several studies have used major and trace element contents, to suggest that the onset of melting is deeper (garnet stability field) and more extensive in the western part of the Archipelago, and less extensive and shallower (spinel stability field) in the eastern sector [1–3,5,24]. Finally, the Sr, Nd, Pb and Hf isotopic composition of the Galapagos lavas indicate that both enriched and depleted mantle components are present in the western and eastern sectors across the 91° W fracture zone [1,5,8]. The exception is the high-$^{3}He/^{4}He$ mantle component found in lavas from Fernandina island ($^{3}He/^{4}He$ 22 to 29 Ra; [19]), which decreases steadily as the distance from Fernandina increases [2].

There is a general agreement that the basalts from a heterogeneous Galapagos plume are diluted with upper mantle melts in the central part of the Archipelago [[1,3], and references therein]. Two different geodynamic models have been proposed to explain this pattern. Richards and Griffiths [25] presented a model that involves entrainment of asthenospheric mantle into a plume subject to bending and velocity shear by the effect of the regional mantle flow. In contrast, Bercovici and Lin [26] proposed that the plume cools by contact with the lithosphere producing gravity currents that cause the plume to take on a mushroom shape, with the hot asthenosphere being entrained in the center, while the plume component is located at the colder margins of the plume.

3. Sampling and analytical techniques

3.1. The data considered in this study include

1) A compilation of all published major, trace element, and isotopic compositions reported for lavas with MgO ≥5 wt.% from the Galapagos Archipelago. This compilation comprises: data from the GEOROC database, the latest published data from the literature not yet in the database, and our own new unpublished data.
2) New sampling of historic to Holocene lavas from numerous volcanoes and islands from the Galapagos Archipelago. Most of the selected samples are younger than 50,000 year old, dated by surface exposure techniques using cosmogenic ^{3}He [2,27–29].

The composition and the young ages of the samples provide a "present-day" picture of the distribution of the compositionally distinctive sources beneath the Archipelago. The dataset reported in Table 1 is only a summary of selected representative samples from each island. The complete dataset is presented in Table 1 of the Supplementary Information.

Major and trace element data reported here were measured by XRF and ICP-MS at the GeoAnalytical Lab, Washington State University. Precisions for most major and trace elements are better than 3% and 10% (2σ), respectively. Sr, Nd and Pb isotopic measurements were carried out on the VG-354 TIMS multi-collector at the Woods Hole Oceanographic Institution. External reproducibilities of the standards were: 16 ppm (2σ, $n=35$) for $^{143}Nd/^{144}Nd$, 26 ppm (2σ, $n=35$) for $^{87}Sr/^{86}Sr$ and 0.05% per amu (2σ, $n=60$) for Pb isotopes. The Sr, Nd and Pb total procedure blanks were less than 40 pg, 70 pg and 150 pg, respectively, and are all negligible. Hf isotopes were measured using the MC-ICPMS Plasma 54 at the Ecole Normale Supérieure in Lyon. The external reproducibility of $^{176}Hf/^{177}Hf$ on replicate Hf standard solutions was better than 30 ppm, and the total procedural Hf blank was less than 25 pg, and thus also negligible (see Supplementary Information for further details on all analytical techniques employed).

4. Results

For this study we selected all samples with MgO contents ≥5 wt.%. All of the lavas are basalts, mostly tholeiitic with only a few alkali basalts. SiO_2 contents and Mg# range from 51.9 to 44.19 wt.% and from 0.76 to 0.40, respectively. The Mg# indicates that most of the samples have undergone fractional crystallization and some have been affected by olivine accumulation (Fig. 1).

We divide the lavas from the Galapagos Archipelago into two main groups: The "western group", formed by basalts erupted from large shield volcanoes (volcanoes on Fernandina and Isabela Islands) close to the leading edge of the plume on an older and thicker lithosphere

Table 1
Major, trace element and isotopic composition of representative Galapagos lavas

Sample ID	NSK97-215	NSK97-238	NSK97-252	NSK97-254	SG93-19	GI92-10	GI92-1	SN 91-60	GI92-16	GI92-18	GI92-19	W95-84	SKV98-108	SKV98-101
Island/volcano	Fernandina	Santiago	San Cristobal	San Cristobal	Floreana	Cerro Azul	Santa Cruz	Sierra Negra	Alcedo	Darwin	Ecuador	Wolf	Pinta	Marchena
Lat. south	0 22.59	0 14.25	0 43.54	0 45.82	1 13.722	0 58.97	0 44.54	0 56.30	0 23.51	0 12.70	0 1.57	0 0.08	0 36.52	0 21.43
Long. west	91 33.93	90 51.03	89 24.63	89 27.31	90 25.465	91 26.63	90 17.53	90 56.30	91 13.15	91 23.10	91 31.14	91 0.30	90 44.41	90 32.18
SiO_2	48.54	48.40	47.30	47.44	46.70	48.39	47.44	48.97	49.64	48.80	47.93	48.58	48.53	48.73
Al_2O_3	13.95	14.85	16.77	16.40	14.16	13.97	16.13	14.13	14.00	16.74	14.32	15.21	16.84	14.42
TiO_2	2.72	2.13	1.01	0.98	1.74	3.73	1.72	3.48	3.06	2.58	2.29	2.88	2.04	2.51
FeO	10.42	10.67	8.83	9.04	9.49	13.69	10.60	13.29	12.36	10.05	11.00	10.97	9.13	12.37
MnO	0.175	0.178	0.165	0.170	0.176	0.223	0.171	0.21	0.204	0.164	0.170	0.18	0.15	0.20
CaO	10.68	10.25	12.37	11.55	11.25	9.90	9.84	10.59	10.82	12.39	9.90	11.20	12.77	11.49
MgO	10.39	10.22	11.17	11.80	13.64	5.31	10.55	5.62	6.11	6.07	10.90	7.09	6.96	6.31
K_2O	0.36	0.31	0.12	0.19	0.48	0.78	0.22	0.50	0.50	0.32	0.52	0.50	0.53	0.32
Na_2O	2.49	2.74	2.16	2.31	2.17	3.59	3.08	2.85	2.91	2.64	2.69	3.05	2.79	3.38
P_2O_5	0.269	0.242	0.104	0.112	0.190	0.433	0.255	0.36	0.408	0.240	0.278	0.35	0.26	0.26
Total	100.00	100.00	100.00	100.00	100.00	100.00	100.00	100.00	100.00	100.00	100.00	100.00	100.00	100.00
XRF														
Ni	226	241	211	259	336	27	236	40	44	56	265	89	61	38
Cr	643	495	481	479	828	46	406	101	98	152	499	248	78	132
Sc	35	34	40	40	34	30	30	30	38	35	27	28	35	44
V	327	246	228	210	264	422	198	385	351	309	226	343	247	335
Ba	40	27	28	44	145	160	0	102	50	24	95	58	124	41
Rb	7	5	3	3	9	16	2	8	8	3	10	3	8	3
Sr	302	234	173	173	338	374	374	298	284	382	344	374	340	221
Zr	135	139	66	67	93	226	158	192	180	155	150	216	143	164
Y	24	29	21	21	22	39	26	36	35	26	25	34	26	39
Nb	18.3	11.1	5.2	6.5	16.2	40	6.2	27.6	21.5	12.8	22.1	17.3	20.9	12.5
Ce	22	26	9	14	26	60	50	29	40	38	38	51	34	23
ICPMS														
Cs	0.06	0.05	0.02	0.04	0.14	0.16	0.03	0.11	0.09	0.06	0.11	0.06	0.06	0.05
Rb	5.96	5.09	1.21	2.28	9.42	14.66	2.25	9.8	7.94	3.61	9.21	5.9	8.6	5.16

Ba	73.47	48.64	23.89	38.49	180	178.98	34	120	85	44	120	60	130	51
Th	1.05	0.76	0.24	0.37	0.89	2.48	0.37	1.64	1.25	0.66	1.27	1.03	1.66	0.73
U	0.30	0.21	0.06	0.10	0.17	0.68	0.09	0.48	0.3	0.18	0.28	0.35	0.39	0.21
Nb	16.89	9.60	3.57	4.94	16.14	35.00	5.71	26.97	21.04	11.9	20.54	15.74	19.98	10.78
Ta	1.24	0.65	0.25	0.31	0.91	2.32	0.36	1.89	1.35	0.8	1.2	1.14	1.39	0.76
La	11.83	9.00	3.38	4.31	11.99	26.32	7.92	19.03	15.78	11.52	15.73	15.74	15.69	10.01
Ce	27.00	20.96	8.46	9.53	21.86	54.42	20.5	42.35	35.45	26.76	32.27	37.81	33.48	24.70
Pb	1.15	1.07	0.90	0.75	1.72	2.06	0.89	1.43	2.9	2.27	1.68	1.38	0.95	0.85
Pr	3.66	2.99	1.31	1.36	2.69	6.91	3	5.53	4.76	3.68	4.09	5.22	4.29	3.62
Sr	289.08	229.61	173.67	167.06	338	377.61	374	308	284	382	344	388	349	235
Nd	17.11	14.86	6.79	6.58	11.88	30.59	14.62	25.68	22.19	17.43	18.84	24.56	19.68	18.46
Hf	3.35	3.53	1.65	1.54	1.85	5.72	3.37	5.09	4.46	3.36	3.36	5.46	3.78	4.39
Sm	4.88	4.90	2.40	2.18	3.39	8.01	4.37	7.22	6.71	5.2	5.23	7.1	5.36	6.07
Eu	1.78	1.79	0.96	0.89	1.22	2.71	1.64	2.52	2.32	1.89	1.81	2.49	1.94	2.23
Gd	5.09	5.61	3.16	2.84	3.69	8.00	4.48	7.76	6.94	5.36	5.22	7.4	5.62	7.33
Tb	0.87	0.94	0.61	0.55	0.66	1.33	0.84	1.31	1.23	0.89	0.89	1.24	0.95	1.29
Dy	5.13	5.86	4.08	3.87	4.14	7.83	5.17	7.56	7.2	5.29	5.12	7.06	5.51	7.65
Y	24.32	29.18	22.96	22.08	22.46	39.40	26.89	37.05	35.59	25.42	25.99	34.04	26.31	40.25
Ho	0.99	1.12	0.89	0.83	0.82	1.55	1.04	1.47	1.39	1.01	0.99	1.37	1.08	1.56
Er	2.46	2.93	2.56	2.37	2.41	3.88	2.9	3.74	3.71	2.7	2.67	3.36	2.71	4.10
Tm	0.34	0.39	0.37	0.34	0.31	0.54	0.4	0.51	0.5	0.35	0.35	0.46	0.37	0.57
Yb	2.00	2.37	2.36	2.32	1.85	3.22	2.38	3.04	2.94	2.01	2.04	2.71	2.2	3.41
Lu	0.29	0.35	0.37	0.36	0.3	0.48	0.38	0.45	0.44	0.29	0.3	0.4	0.33	0.52
Sc	33.62	32.35	45.35	41.56		34.13		34.4				36.9	32.4	40.23
$^{87}Sr/^{86}Sr$	0.703264	0.703036	0.702991	0.703086	0.703446	0.703321	0.702952	0.703397	0.703174	0.702856	0.703200	0.702747	0.703288	0.702843
$^{143}Nd/^{144}Nd$	0.512922	0.512998	0.513041	0.513042	0.512945	0.512934	0.513099	0.512925	0.512962	0.513020	0.512951	0.513041	0.512909	0.513028
$^{176}Hf/^{177}Hf$	0.283054	0.283033	0.283144	0.283139				0.283034		0.283068	0.283051	0.283104	0.283012	0.283109
$^{206}Pb/^{204}Pb$	19.109	19.015	18.704	18.783	19.614	19.337	18.521	19.357	19.116	18.810	19.304	18.897	19.156	18.893
$^{207}Pb/^{204}Pb$	15.548	15.561	15.555	15.546	15.599	15.561	15.497	15.591	15.552	15.536	15.600	15.542	15.594	15.563
$^{208}Pb/^{204}Pb$	38.758	38.657	38.386	38.416	39.300	38.955	38.038	39.022	38.699	38.268	39.059	38.377	39.003	38.500
$^{208*}/^{206*}$	0.947	0.946	0.948	0.943	0.953	0.945	0.929	0.950	0.940	0.925	0.959	0.928	0.967	0.941

For a complete dataset of the samples analyzed See Table 1 in the Supplementary Information.

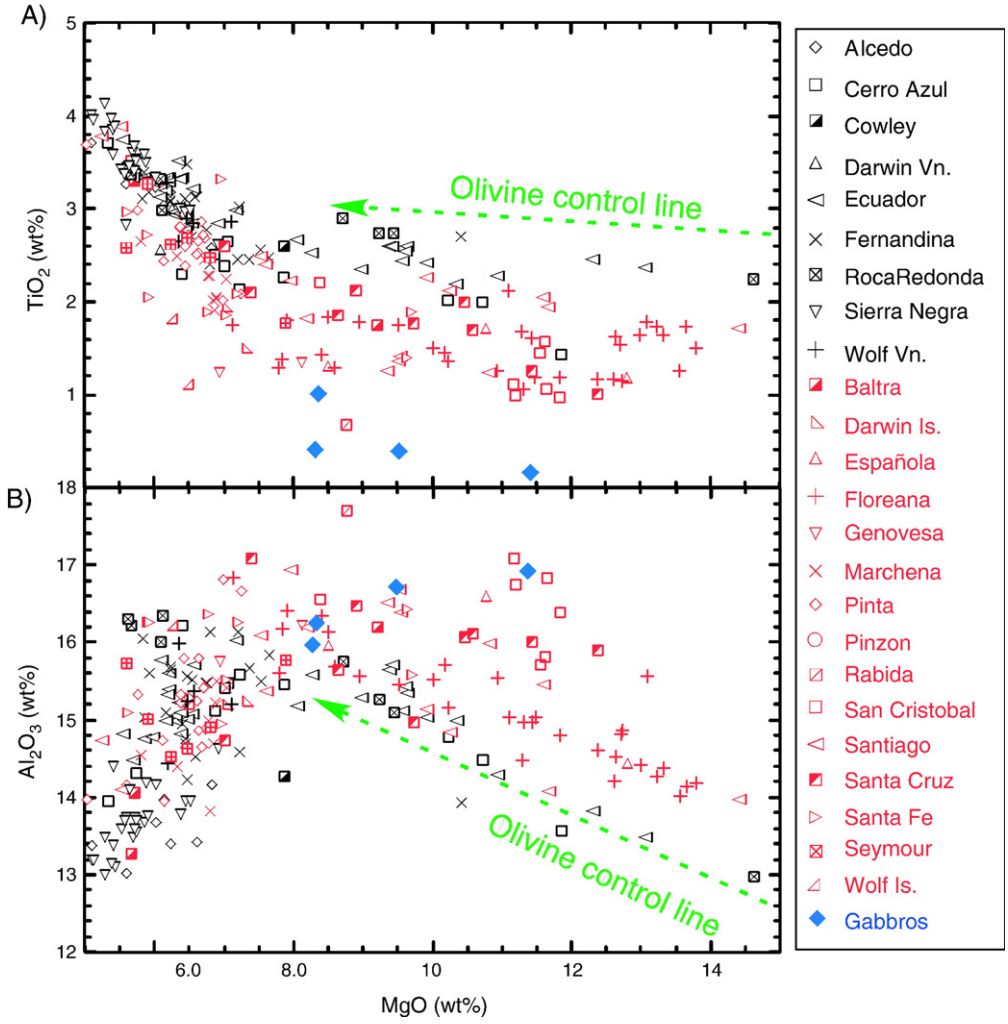

Fig. 1. A) TiO_2 and B) Al_2O_3 versus MgO contents of Galapagos lavas. The analyses used are a compilation of all the published data available through the GEOROC database complemented with the data presented in this study. Only samples with MgO content > 5 wt.% have been considered in our work. Dashed arrow indicates the olivine control line. We also plot the median for gabbros from Annieopsquotch [30] the oceanic crust (two median values are presented one for "protoliths" and one for "strips") [31] and Oman [[32] and reference therein]. Symbols in black and red represent lavas from the "western" and "eastern" groups respectively.

located to the west of the 91° fracture zone [12,14,28]. The second group, the "eastern group", represents lavas erupted from small cones and vents located in islands further away from the leading edge of the plume on a relatively thin and young lithosphere. Most of the lavas in the eastern group are located to the east of the 91° fracture zone, with the exception of the basalts from Darwin and Wolf Islands, which actually erupted to the west of the fracture zone. It is important to emphasize that the present-day eruption rates are different between both groups, with the western group having higher eruption frequency than the eastern group [2,3,28].

The compilation of all the existing data reveals that even though lavas from both groups share similar ranges in Sr, Nd, Pb, and Hf isotopes (with the eastern group displaying a larger range), they have important differences in their major and trace element compositions. Lavas from the eastern group range from similar to lower TiO_2 and higher Al_2O_3 contents, lower incompatible trace element abundances, and lower MREE/HREE ratios (e.g., Sm/Yb, Hf/Lu) than those from the western group at similar MgO contents (Figs. 1 and 2). Moreover, while lavas from the western volcanoes are characterized by positive Nb and Ti anomalies, and negative K and Pb anomalies in primitive-mantle-normalized plots, many basalts from the eastern group are distinguished by negative Th anomalies, positive Ba, Sr and small Eu anomalies, and small or no negative

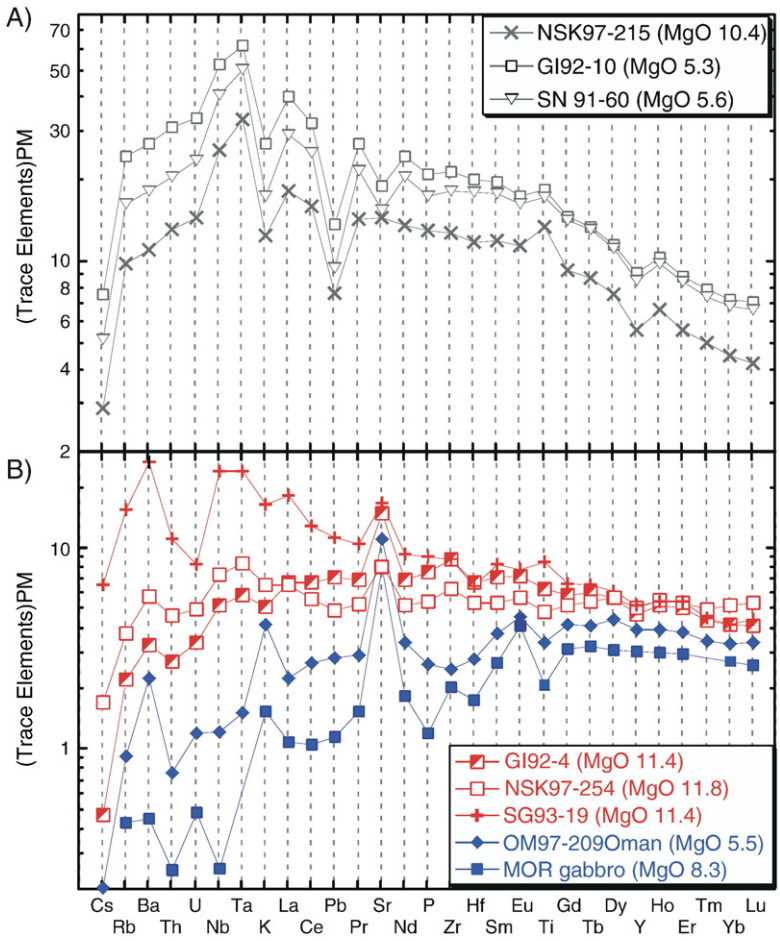

Fig. 2. Primitive mantle-normalized diagram for representative samples from the Galapagos Archipelago: A) The western region (Fernandina, Cerro Azul and Sierra Negra volcanoes). B) The eastern region (Floreana, Santa Cruz and San Cristobal Islands). For comparison, we included representative analyses of gabbros from the oceanic crust [31] and Oman [[32] and reference therein]. Normalizing values are from McDonough and Sun, [55]. Symbols as in Fig. 1.

anomalies for K and Pb. These anomalies represent ratios involving pairs of trace elements with similar incompatibilities, which are not easily fractionated during mantle melting. Thus, high Ba/Th, K/La, Sr/Nd (~Sr/Sr*), Eu/Eu* and Pb/Nd ratios characterize the source of many lavas from the eastern group, while high Ti/Gd and Nb/La (~Nb/Nb*), and low K/La and Pb/Nd ratios distinguish the source of basalts from the western group (Fig. 2, and Supplementary Information Fig. 1 and Table 2).

To avoid the problems of temporal variation between lavas from different volcanoes/islands, the lack of inter-laboratory calibrations, and the differences in analytical techniques inherited in the compilation of all the existing Galapagos data, we plot key trace element ratios using only our own new data set (Fig. 3). Most selected samples are less than 50 ka old, with the exception of three samples from Floreana (100–200 ka) and two samples from Santa Cruz, (100 ka and 500 ka), providing a present-day picture of the compositional variation across the archipelago. All samples were analyzed in the same laboratory, and batches of samples from both eastern and western groups were analyzed during the same analytical sessions. Our data confirm the observations made using the compilation of all the existing data, and demonstrate that the different trace element compositions between eastern and western groups are not an artifact of the data compilation.

The relative high Ba/Rb, Ba/Th (Th/Th*), K/La, Sr/Nd, Eu/Eu* and Pb/Nd ratios in some lavas from the eastern group resemble those of plagioclase-rich cumulates from the oceanic crust and ophiolite complexes (hereafter referred to as the “plagioclase-rich gabbro” signature). Therefore, we compared the composition of

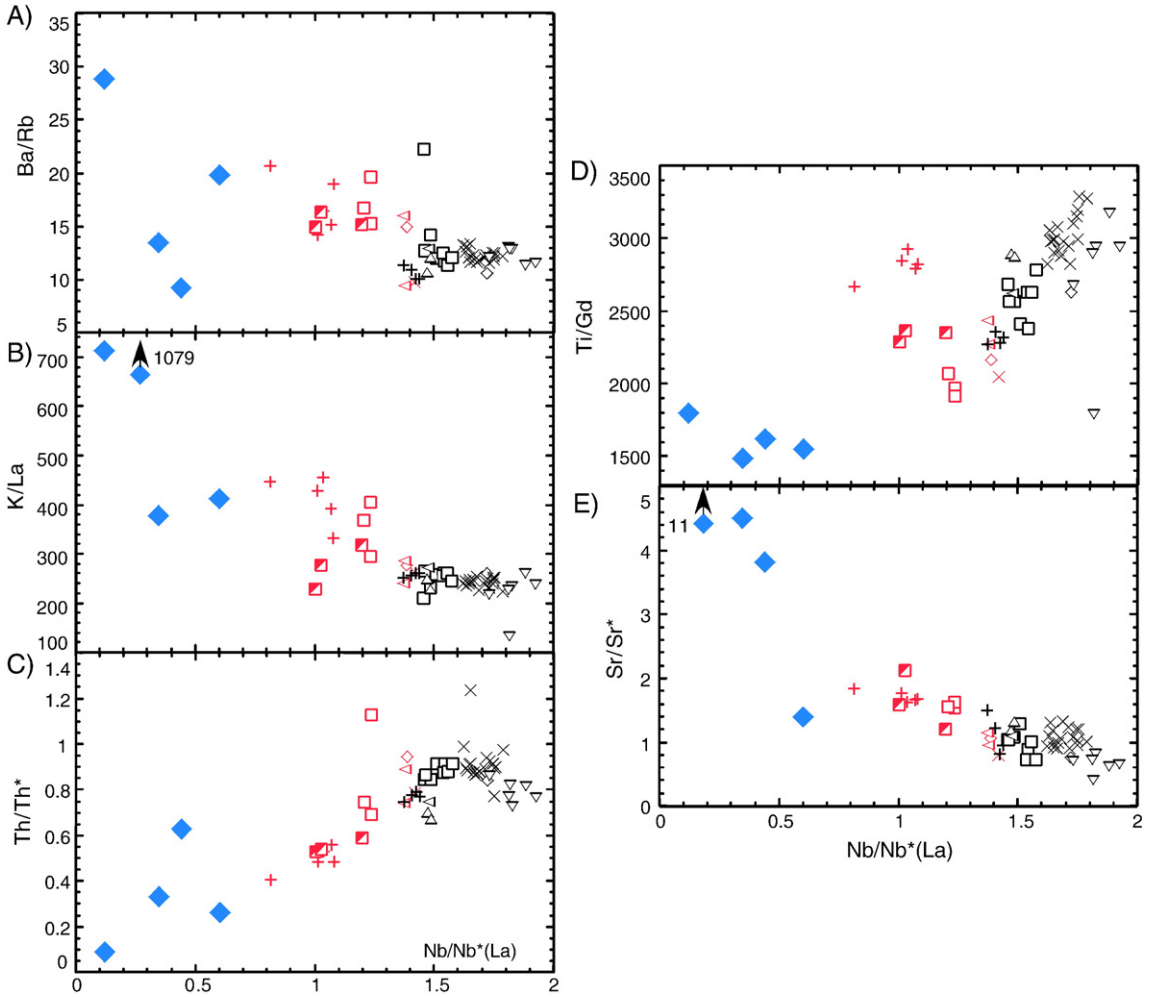

Fig. 3. Ti/Gd, Ba/Rb, K/La, Sr/Sr*, and Th/Th* versus Nb/Nb*(La) for individual Galapagos lavas reported in Table 1 of the Supplementary Information. Note that most of the samples are younger than 50 ka with the exception of three samples from Floreana (100–200 ka) and two samples from Santa Cruz, (100 ka and 500 ka). We plot the median for gabbros from Annieopsquotch [30] the oceanic crust [31] and Oman [[32] and reference therein]. Nb/Nb*(La)=[Nb/((Ba+La)/2)] and Sr/Sr*=[Sr/((Pr+Nd)/2)] and Th/Th*=[Th/((Ba+La)/2)] using normalized values. Normalizing values are from McDonough and Sun [55]. Symbols as in Fig. 1.

the Galapagos lavas with the median composition of gabbroic cumulates from ophiolites and the oceanic crust [30–32] and reference therein]. Figs. 1, 2 and 3 (see also Supplementary Information Fig. 1 and Table 2) clearly show that lavas from the eastern group have intermediate trace element compositions between those from the western group and the plagioclase-rich cumulates.

The Sr, Nd, Pb, Hf and He isotope data of lavas from the Archipelago have been discussed extensively [1,2,5,6,8,28,33,34]. Our compilation confirms the conclusions previously reached in those papers. Namely, most of the isotopic variation within the archipelago occurs between volcanoes/islands, and generates a geographic distribution of the isotopic variations that defines a horseshoe pattern [1,2,5,33,34]. Four main components are needed to bracket the isotopic composition of lavas from the archipelago: a MORB component defined by the Genovesa lavas, two enriched components defined by Floreana and Pinta basalts, and the high-$^{3}He/^{4}He$ component characterized by Fernandina lavas. Two main observations arise from dividing the Archipelago into the western and eastern groups: 1) Lavas from the eastern group tend to have higher $^{87}Sr/^{86}Sr$ at similar $^{143}Nd/^{144}Nd$ than those from the western group. To illustrate this observation Fig. 4 shows a third-order polynomial fit to the data for the western group lavas on the $^{143}Nd/^{144}Nd$–$^{87}Sr/^{86}Sr$

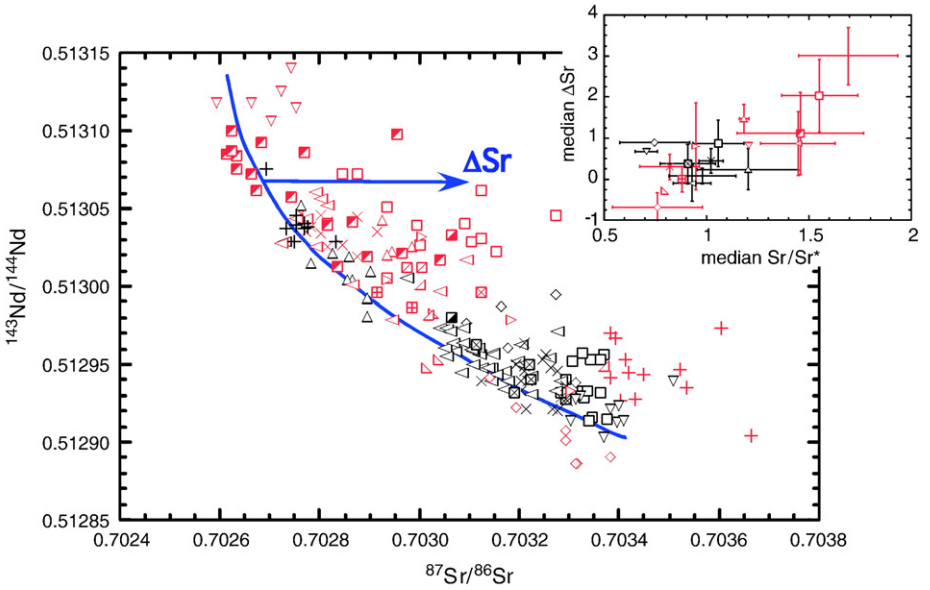

Fig. 4. $^{143}Nd/^{144}Nd$ versus $^{87}Sr/^{86}Sr$. The analyses used are a compilation of all the published data available through the GEOROC database complemented with the data presented in this study. The curve is the fitted polymomial of the third order to the data of the western group lavas. ΔSr is the deviation in $^{87}Sr/^{86}Sr$ of each sample to that curve at equal $^{143}Nd/^{144}Nd$. $\Delta Sr = \{^{87}Sr/^{86}Sr - [2.969 - 4.4170 \times Nd + 8327.8535 \times (Nd - 0.51299)2 + 51{,}322{,}354 \times (Nd - 0.51299)3]\} \times 10{,}000$. The inset shows a plot of the ΔSr versus Sr/Sr*. We used the median for Sr/Sr*, ΔSr from each island/volcano. Error bars represent 2σ standard errors; we did not report the error bars when the number of samples analyzed per island/volcano was ≤3. Samples with no reported major element compositions were not considered in the calculation of the median to avoid the effect of crystal fractionation. Sr/Sr* = [Sr/((Pr+Nd)/2)] using normalized values. Normalizing values are from McDonough and Sun [55]. Symbols as in Fig. 1.

diagram; the deviation from this curve toward higher $^{87}Sr/^{86}Sr$ at a given $^{143}Nd/^{144}Nd$ for each sample is referred to as ΔSr. The ΔSr is not only higher in lavas from the eastern group, but also correlates with the Sr/Sr* ratios (Fig. 4 inset). 2) $^{3}He/^{4}He$ values are higher in lavas from the western group, reaching a maximum in basalts from Fernandina Island. Also, $^{3}He/^{4}He$ ratios define a positive correlation with Ti/Gd and Nb/La ratios, suggesting that high Ti/Gd and Nb/La ratios are typical of the mantle source carrying the high-$^{3}He/^{4}He$ signature (see [2] and Fig. 5).

5. Discussion

5.1. Compositional variation across the Archipelago; plume, entrained MORB and lithospheric signatures

Geological, geochemical and geophysical information point to the existence of an upwelling thermal plume beneath the Galapagos Archipelago. The Rayleigh wave tomographic study of Villagomez et al. [14] shows a continuous low-velocity volume beneath the western volcanoes (Fernandina and Isabella Islands), which flattens against the base of the "high-velocity lid", tilts in a northerly direction and spreads eastward and westward. These results are consistent with the anomalously thin mantle transition zone observed beneath the western volcanoes [12], the age progression of the oldest lavas dated from each volcano, from young in the west to old in the east [1,2,21], and with the high eruption frequency and the high $^{3}He/^{4}He$ ratios measured for Fernandina basalts [2,28].

The interaction between plume melts and MORB most likely controls the isotopic composition of the lavas from both, the western and eastern, regions ([1,2,5]). Fluid dynamic models have shown that depleted upper mantle can be entrained into the plume flow either by significant lateral entrainment of ambient mantle into the plume conduit, or as an ambient mantle viscously coupled to the plume flow [35]. However, even though the lavas from both regions share similar range in Nd, Hf and Pb isotopes, their trace element compositions are significantly different. Such differences in the basalt compositions are characterized by a decrease in the Nb/Nb* and Ti/Gd ratios, and an increase in the Ba/Th, K/La, Sr/Sr*, Eu/Eu* and Pb/Nd ratios from west to east (Fig. 3 and Supplementary Information Fig. 1 and Table 2). For example, when lavas from Wolf and Darwin volcanoes (western group) are compared with lavas from Santa Cruz and San Cristobal Islands (eastern group), both suite of basalts have similar Nd, Hf and Pb isotopic compositions (e.g., similar Nd isotopes in Fig. 4), but

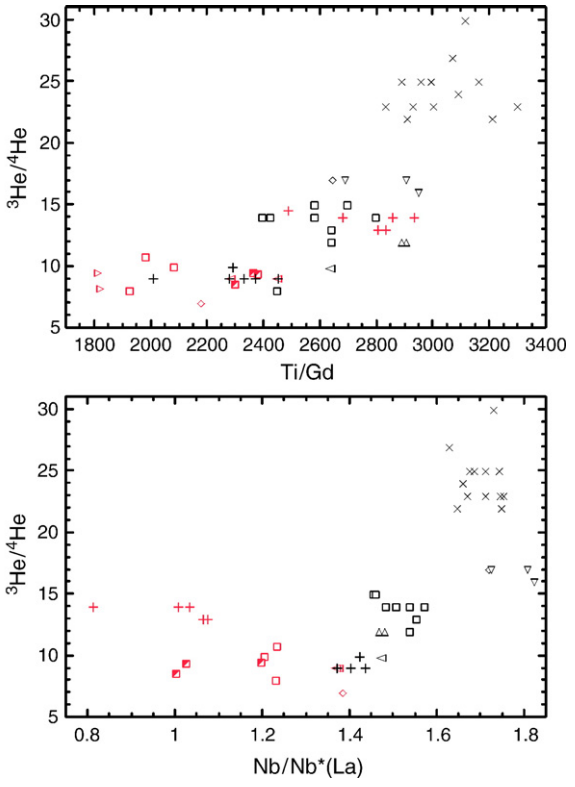

Fig. 5. $^{3}He/^{4}He$ versus Ti/Gd, and Nb/Nb*(La) for Galapagos lavas. Data from Kurz and Geist [2], Kurz unpublished data, and this study. Symbols as in Fig. 1.

lavas from Santa Cruz and San Cristobal have a "plagioclase-rich gabbro" signature in their trace element composition and high ΔSr that are absent from Wolf and Darwin's basalts (Figs. 3, 4). Similar observations can be made by comparing lavas from Sierra Negra and Cerro Azul volcanoes (western group), with lavas from Floreana Island (eastern group).

The $^{3}He/^{4}He$ ratios and the ΔSr represent the main isotopic difference between lavas from the western and eastern groups. $^{3}He/^{4}He$ correlates with Ti/Gd and Nb/La ratios (Fig. 5), and all three ratios decrease with increasing distance from Fernandina. These correlations suggest that the high Ti/Gd and Nb/La ratios are typical of the plume mantle source that carries the high $^{3}He/^{4}He$ signature. In contrast, the ΔSr is characteristic of lavas with a "plagioclase-rich gabbro" signature. This is best exemplified by the correlation of Sr/Sr* with ΔSr in basalts from the eastern group (Fig. 4 inset). Therefore, the process responsible for the generation of the "plagioclase-rich gabbro" signature affected both, the trace element and the Sr isotopic composition of the lavas.

The variations in Nb/Nb*, Ti/Gd, Ba/Th, K/La, Sr/Sr*, Eu/Eu* and Pb/Nd ratios between lavas from the eastern and western groups have to be controlled by either variations in the mantle source compositions or some type of interaction process within the lithosphere. The similar incompatibility of the trace elements used in each ratio precludes significant variations of these ratios during mantle melting. Furthermore, plagioclase accumulation during magma differentiation could produce basalts with trace element ratios similar to those observed in lavas from the eastern group. However, inspection of thin sections from samples with "plagioclase-rich gabbro" signature indicates that those samples have less than 1% plagioclase phenocrysts. Therefore, plagioclase accumulation is not the process responsible for the unusual trace element ratios observed in many basalts from the eastern group. In contrast, plagioclase fractionation during basalt differentiation could erase the "plagioclase-rich gabbro" signature, making it difficult to determine whether originally a lava had such a signature or not (see an example in Fig. 2 of the Supplementary Information). Basalts from the northern area of the archipelago (e.g., lavas from Pinta, Marchena, Wolf and Darwin Islands) do not show the "plagioclase-rich gabbro" signature in their trace element compositions; because most of these lavas are quite evolved, it is not clear whether the lack of such a signature is an original characteristic of these lavas, or is related to plagioclase fractionation.

5.2. The origin of the "plagioclase-rich gabbro" signature

Two main hypotheses have been proposed to explain the "plagioclase-rich gabbro" signature in oceanic island basalts: 1) the presence of an ancient recycled plagioclase-rich cumulate (now eclogite), as a component intrinsic to the mantle plume [36–38], and 2) the interaction of basalts with plagioclase-rich cumulate during melt percolation through the oceanic lithosphere [39–41].

The "plagioclase-rich gabbro" signature in the Galapagos lavas cannot be explained by melts generated from either an entrained upper mantle component, or an ancient recycled plagioclase-rich gabbro component within the plume. Melting of the upper mantle will produce basalts similar to MORB, which lack the "plagioclase-rich gabbro" signature. Meanwhile, melts generated from an ancient recycled plagioclase-rich cumulate (now eclogite) within the plume will be characterized by low $^{206}Pb/^{204}Pb$ compared to those of present-day MORB. However, the Galapagos lavas with a "plagioclase-rich gabbro" signature have $^{206}Pb/^{204}Pb$ that is either very similar to, or much higher (as in the case of Floreana lavas) than those

of present-day MORB. Thus, the only alternative explanation for the origin of the "plagioclase-rich gabbro" signature in the Galapagos lavas is the interaction of basalts with plagioclase-rich cumulates during melt percolation through the oceanic lithosphere.

There seems to be a geographic distribution of lavas with a "plagioclase-rich gabbro" signature within the archipelago. Most of these lavas are located to the east of the 91° fracture zone, within the central-eastern and southeastern sectors of the archipelago. Three main factors seem to be associated with the geographic distribution of this group of lavas: 1) The composition of the lavas, 2) the variation in the magmatic flux passing through the lithosphere, and 3) the variation of the lithospheric thickness. First, the low incompatible trace element contents of the magmas generated from the depleted mantle source erupting in the central-eastern and southeastern sectors [1,5] make the lavas more susceptible to modification during melt-cumulate interaction than incompatible trace element enriched melts generated from the mantle plume. Second, the central-eastern and southeastern sectors are characterized by a low present-day magmatic flux through the lithosphere, as indicated by their low eruption frequency, which decreases with increasing distance from Fernandina and Isabela Islands [2,3,28]. Finally, seismic information indicates that the "high-velocity lid" to the east of the 91° W fracture zone thickens from north to south with increasing distance from the GSC [14]. The combination of a thicker lithosphere and low magmatic flux will effectively reduce the melt to rock ratio creating an environment conducive to the chemical modification of the lava during transport through the lithosphere. Therefore, the increase in the abundance of lavas with depleted trace element compositions combined with the thickening of the lithosphere and the decreasing magma flux would result in basalts with a "plagioclase-rich gabbro" signature within the central-eastern and southeastern regions of the archipelago.

Most of the plagioclase-rich cumulates beneath the central-eastern region of the archipelago originated from the crystallization of melts probably at the GSC during the time the Galapagos plume was centered or close to the ridge. Studies of ophiolites suggest that the crust–mantle transition zone beneath ocean ridges is one of the possible areas where such cumulates may be stored. This zone, located between the underlying residual peridotite and the dominantly gabbroic crustal section, is a diffuse area formed by successive stages of basaltic melt injections that extends sideways from the ridge axis for tens of kilometers. The composition of the gabbroic rocks in this zone indicates that they are cumulates formed by partial crystallization of basalts, and demonstrates that plagioclase-rich cumulates can form far below the level of magmatic neutral buoyancy [42–46]. Multichannel seismic studies of the crust–mantle transition zone beneath mid-ocean ridges show that this zone is characterized by low seismic velocities, suggesting the presence of low melt fractions (a maximum of a few percent), and inefficient heat removal [47–49]. The interaction of the Galapagos plume with the GSC would certainly enhance and probably extend the crust–mantle transition zone between the archipelago and the ridge.

Direct assimilation or partial melting of plagioclase-rich cumulates followed by mixing with plume melts cannot account for the observed major and trace element composition of the lavas with a "plagioclase-rich gabbro" signature. A direct assimilation process would require an unreasonably large proportion of digested cumulate material to produce the trace element composition of the lavas from the eastern group (see Supplementary Information Fig. 3). In addition, the existing experimental data indicate that melt generated by partial melting of gabbro have high SiO_2 content [[50], and references therein], but Galapagos lavas with "plagioclase-rich gabbro" signature have relatively low SiO_2 contents. Therefore, neither assimilation nor partial melting of gabbro cumulate is the process responsible for the trace element composition of lavas in the eastern region. As will be shown below, diffusive interaction between plagioclase-rich cumulates and percolating basalts can explain the observed "plagioclase-rich gabbro" signature.

5.3. A melt-cumulate diffusive interaction model

The basic idea behind this model is that cations of different size and charge diffuse at different rates in plagioclase, giving rise to kinetic fractions among the incompatible trace elements (e.g., diffusivities of Sr^{2+} and Pb^{2+} are significantly larger than those of REE^{3+} in plagioclase; see Supplementary Information Table 3). As a first step towards testing this hypothesis, we consider a simple end member case of a troctolitic mush (plagioclase+olivine+melt) in which the variations in the incompatible trace element content in the interstitial percolating melt are due only to diffusive exchange between the melt and its surrounding minerals. Since olivine does not significantly contribute to the incompatible trace element budget, only providing a dilution effect, our model evaluates the diffusive interaction between a melt and a single solid cumulate phase, plagioclase. For simplicity, we neglect the effects of crystal dissolution, precipitation or crystallization that

may arise during crystal–melt diffusive re-equilibration in a partially molten system [51,52]. A more general case considering melt percolation, diffusive exchange, and dissolution-re-precipitation processes between gabbro (plagioclase+clinopyroxene+olivine) and interstitial melt will be the focus of a future paper.

Since the exact solutions to the problem of diffusive re-equilibration between a crystal and a well-stirred melt pocket (plagioclase+melt) in a spherical, cylindrical, or one-dimensional setup are rather complicated [53], we use a simple approximate solution to the diffusion equations in a finite crystal–melt geometry [51]. This simple solution was obtained by approximating the concentration gradient at the crystal–melt interface using boundary layer theory. In the model, the solid is assumed to be homogeneous in composition at the onset of melt-cumulate interaction. During the interaction, the interface between the solid and the melt is assumed to be in chemical equilibrium at all times; the mineral grains do not deform, and the concentrations in the interior of the grains are only controlled by diffusion. Furthermore, the diffusion in the melt is assumed to be instantaneous. In the model presented here, the variation of the trace element concentration in the melt with time, $C_f(t)$, is given by:

$$C_f(t) = C_f^{\infty} + (C_f^0 - C_f^{\infty})\exp(-\alpha_K t) \quad (1a)$$

$$C_f^{\infty} = \frac{\rho_f \phi C_f^0 + \rho_s(\phi-1)C_s^0}{\rho_f \phi + \rho_s(\phi-1)K_D} \quad (1b)$$

$$\alpha_K = \frac{3D_s}{r^2}\frac{[\rho_f \phi + \rho_s(\phi-1)K_D]}{\rho_f \phi} \quad (1c)$$

where C_f^0 and C_s^0 are the initial trace element concentrations in the melt and solid, respectively; C_f^{∞} is the equilibrium trace element concentration in the melt; ϕ is the volume fraction of the melt (porosity); K_D is the solid-melt partition coefficient; r is the radius of the mineral grain; D_s is the diffusion coefficient in the solid phase, t is time; and ρ_s and ρ_f are the densities of the solid and the melt, respectively.

The case presented here considers a melt with a composition similar to a primitive MORB interacting with plagioclase-rich cumulate crystallized from a melt having relatively higher incompatible trace element contents, higher Sm/Yb ratios and $^{87}Sr/^{86}Sr$ ratios. Mixing of plume and upper mantle melts at either the GSC or at the leading edge of the plume in the western sector of the archipelago could easily be responsible for the generation of the enriched melts that produced the cumulates [54]. We performed a model run using the parameter values listed in Table 3 of the Supplementary Information. We assumed a troctolite comprised of an equal proportion of olivine and plagioclase. Previous studies of the crust–mantle transition zone constrain the grain size of the crystal phases to 1–2 mm [45], the melt to rock ratio to 1–2%, and the temperature to approximately 1200 °C [47]. We further assumed that the temperature remained constant at 1200 °C, consistent with the inferred inefficient heat removal from the transition zone [47].

Fig. 6 displays the results of this simple diffusive interaction model, which can easily explain the composition of the erupted lavas; in this specific example the composition of a basalt from San Cristobal Island is reproduced. Hence, diffusive interaction between oceanic basalts and plagioclase-rich cumulates can produce significant changes in the trace element composition of the percolating lavas. During melt-cumulate interaction, the Ba/Th, K/La, Sr/Nd, Eu/Eu* and Pb/Nd ratios in the melt radically diverge from those initially produced during mantle melting. The trace elements will diffuse from the cumulate into the melt in an attempt to reach equilibrium. The larger diffusion coefficients of Ba, K, Sr, Eu^{+2}, and Pb in plagioclase compared to those of Th, La Nd, and Gd, will ultimately generate a "plagioclase-rich gabbro" signature equivalent to that observed in lavas from the central-eastern region of the archipelago. Furthermore, because the depleted percolating melt has a lower $^{87}Sr/^{86}Sr$ ratio than the cumulate, the diffusive interaction process will also increase the $^{87}Sr/^{86}Sr$ ratios in the melt at a rate that is significantly faster than that required to modify the $^{143}Nd/^{144}Nd$ ratios, resulting in a high ΔSr values. Thus, contemporaneous variation in the ΔSr and the Sr/Sr* during melt-cumulate diffusive interaction would provide an explanation for the observed ΔSr–Sr/Sr* correlation defined by the Galapagos lavas with "plagioclase-rich gabbro" signature (Fig. 6B).

As shown in Eqs. (1a)–(1c), the compositions of the percolating melt and the cumulate, the interaction time, the grain size, and the melt to cumulate ratio (or porosity) are among the most important factors influencing the results of our model. Clearly, the larger the chemical disequilibrium between the percolating melt and the cumulate, the more susceptible the melt will be to the diffusive interaction. For example barium, due to its lower diffusion coefficient in plagioclase compared to those of K, Sr, and Pb, would require either a longer interaction time or a larger chemical disequilibrium between the percolating melt and the cumulate to produce an anomaly similar to those of the other elements. This process can also explain the observation that most Galapagos lavas with "plagioclase-rich gabbro"

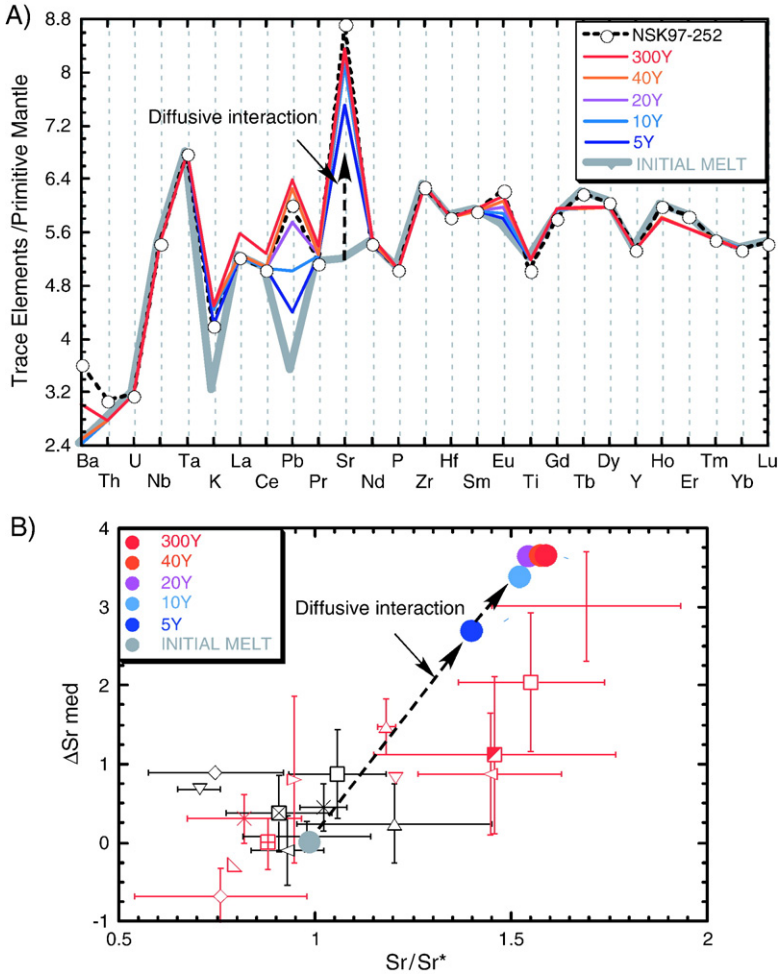

Fig. 6. Calculated results of diffusive interaction between a melt with a composition similar to a primitive MORB interacting with plagioclase-rich cumulate crystallized from a melt with relatively higher incompatible trace element contents, higher Sm/Yb ratios and $^{87}Sr/^{86}Sr$ ratios. The results are displayed as A) Primitve mantle-normalized trace elements and B) ΔSr versus Sr/Sr*. We compare the results of our model with the actual trace element composition of a basalt from San Cristobal Island, NSK97-252. The arrow indicates the direction of progressive diffusive interaction with time. For the example presented here, we assumed a troctolite comprised of an equal proportion of olivine and plagioclase (grain size = 2 mm), melt to rock ratio of 1%, at 1200 °C. We display five different interaction times 5, 10, 20, 40 and 300 years. The input and output data of the model are shown in Table 3, Supplementary Information.

signature do not show significant Eu anomalies. The small positive Eu anomaly in samples with large positive Sr anomalies would suggest that either Eu is present mostly as Eu^{+3}, which has a lower diffusion coefficient than Sr (see Table 3 of the Supplementary Information), or the chemical disequilibrium between the percolating melt and the cumulate is significantly smaller for Eu^{+2} than for Sr. Furthermore, a percolating melt could develop both a positive Sr anomaly and a negative Eu anomaly during diffusive interaction with a plagioclase-rich cumulate. This case requires a percolating melt with lower Sr and higher Eu contents than those of the melt responsible for the generation of the cumulate. This would occur when an incompatible trace element depleted melt, generated in the spinel stability field, interacts with a plagioclase cumulate crystallized from an incompatible trace element enriched melt generated in the garnet stability field. Scenario that is quite likely for the lavas erupted on the central-eastern region of the archipelago. Thus, a precise knowledge of the percolating melt and cumulate compositions, and the partition and diffusion coefficients would be required to determine the interaction time between the melt and the plagioclase cumulate. Even though the interaction time cannot be precisely defined, it is evident from the results of our simple model that very short times, on the order

of a few years, are required to produce the "plagioclase-rich gabbro" signature in the percolating basalt.

Another factor affecting the interaction time is the grain size of the cumulate. Increasing the grain size is equivalent to reducing the surface area over which the diffusive interaction takes place. Thus, the result of increasing grain size will be comparable to decreasing the melt-cumulate interaction time. Increasing the plagioclase grain size will require longer interaction times to achieve the same degree of diffusive exchange. Furthermore, we have to take into account the effect of the melt fraction in our model. Our results indicate that the larger the melt to plagioclase-cumulate ratio, the less pronounced the effects of diffusive interaction on the melt. Seismic data constrain the porosity in the crust–mantle transition zone beneath mid-ocean ridges to, at most, a couple of percent [47–49]. Therefore, the melt to cumulate ratio will be small and the effect of diffusive interaction within the crust–mantle transition zone thus may have a large influence on the trace element and isotope ratios of the percolating melt.

The model presented here assumes that the percolating melt is saturated with plagioclase, and therefore there is only diffusive interaction between the melt and the cumulate without dissolution or re-crystallization of the plagioclase. Interaction of plagioclase-undersaturated melts with plagioclase-rich cumulates would cause the dissolution of plagioclase from the cumulate. Due to the compatible behavior of Sr in plagioclase, dissolution of such mineral would generate an enhanced "plagioclase-rich gabbro" signature in the melt, with an even larger Sr/Sr* anomalies than those produced by simple diffusive interaction processes. The high Al_2O_3 content of the Galapagos lavas with a "plagioclase-rich gabbro" signature suggests that dissolution of plagioclase occurred during the percolation of the lavas through the oceanic lithosphere. Therefore, our simple diffusive interaction model represents a conservative approach to evaluating the melt-cumulate interaction processes that affected the composition of the Galapagos basalts.

6. Conclusions

The Galapagos Archipelago can be divided into two distinct volcanic areas, east and west of the 91° W fracture zone. We find important differences in the compositions of the lavas from both regions. First, the Ti/Gd and Nb/La ratios correlate with $^3He/^4He$, and all three ratios decrease with increasing distance from Fernandina. These correlations suggest that the high Ti/Gd and Nb/La ratios are typical of the plume mantle source that carries the high $^3He/^4He$ signature. Second, there is an increase in the Ba/Th, K/La, Sr/Nd, Eu/Eu*, Pb/Nd ratios, and ΔSr in lavas erupted from west to east across the fracture zone, and from north to south within the eastern region. The high Ba/Th, K/La, Sr/Nd, Eu/Eu*, and Pb/Nd ratios in the Galapagos basalts from the eastern region resemble the composition of plagioclase-rich cumulates from the oceanic crust and ophiolite complexes. The compositions of these lavas can be explained by interaction with plagioclase-rich cumulate during melt percolation through the oceanic lithosphere. We argue that diffusive interaction of basalts with plagioclase-rich cumulates, formed either in the Galapagos Spreading Center or beneath the leading edge of the plume on the western region, are responsible for the observed trace element compositions of lavas in the eastern region.

Acknowledgements

We thank M. Perfit, W. White and J. Sinton for their thoughtful reviews that considerably improved the manuscript. We are grateful to the Charles Darwin Research Station for the logistical support during the field trips to the Galapagos Islands. This work has benefited greatly from discussions with E. Hauri, J. Van Orman and E. Drenkard. The support for this work was provided by the US National Science Foundation.

Appendix A. Supplementary data

Supplementary data associated with this article can be found, in the online version, at doi:10.1016/j.epsl.2007.02.040.

References

[1] W.M. White, A.R. McBirney, R.A. Duncan, Petrology and geochemistry of the Galapagos Islands: portrait of a pathological mantle plume, J. Geophys. Res. 98 (1993) 19533–19563.
[2] M.D. Kurz, D.J. Geist, Dynamics of the Galapagos hotspot from helium isotope geochemistry, Geochim. Cosmochim. Acta 63 (23–24) (1999) 4139–4156.
[3] D.J. Geist, T. Naumann, P. Larson, Evolution of Galapagos magmas: mantle and crustal fractionation without assimilation, J. Petrol. 39 (5) (1998) 953–971.
[4] K. Hoernle, R. Werner, J. Phipps Morgan, D. Garbe-Schönberg, J. Bryce, J. Mrazek, Existence of complex spatial zonation in the Galapagos plume for at least 14 Ma, Geology 28 (5) (2000) 435–438.
[5] K.S. Harpp, W.M. White, Tracing a mantle plume: isotopic and trace element variations of Galapagos seamounts, Geochem. Geophys. Geosyst. 2 (2001) (paper number 2000GC000137).
[6] J.-G. Schilling, D. Fontignie, J. Blichert-Toft, R.H. Kingsley, U. Tomza, Pb–Hf–Nd–Sr isotope variations along the Galapagos Spreading Center (101–83 W): constraints on the dispersal of the

Galapagos mantle plume, Geochem. Geophys. Geosyst. 4 (2003) (paper number 2002GC000495).
[7] D.M. Christie, R.A. Duncan, A.R. McBirney, M.A. Richards, W.M. White, K.S. Harpp, C.G. Fox, Drowned islands downstream from the Galapagos hotspot imply extended speciation times, Nature 355 (1992) 246–248.
[8] J. Blichert-Toft, W.M. White, Hf isotope geochemistry of the Galapagos islands, Geochem. Geophys. Geosyst. 2 (2001) (paper number 2000GC000138).
[9] M.A. Feighner, M.A. Richards, Lithospheric structure and compensation mechanism of the Galapagos Archipelago, J. Geophys. Res. 99 (1994) 6711–6729.
[10] J.P. Canales, G. Ito, R. Detrick, J. Sinton, Crustal thickness along the western Galapagos Spreading Center and the compensation of the Galapagos hotspot swell, Earth Planet. Sci. Lett. 203 (2002) 311–327.
[11] R. Montelli, G. Nolet, F.A. Dahlen, G. Masters, E.R. Engdahl, S.-H. Hung, Finite-frequency tomography reveals a variety of plumes in the Mantle, Science 303 (2004) 338–343.
[12] E.E. Hooft, D.R. Toomey, S.C. Solomon, Anomalously thin transition zone beneath the Galapagos hotspot, Earth Planet. Sci. Lett. 216 (2003) 55–64.
[13] R. Werner, K. Hoernle, U. Barckhausen, F. Hauff, Geodynamic evolution of the Galapagos hot spot system (Central East Pacific) over the past 20 m.y.: constraints from morphology, geochemistry, and magnetic anomalies, Geochem. Geophys. Geosyst. 4 (2003) (paper number 2003GC000576).
[14] D.R. Villagomez, D.R. Toomey, E.E. Hooft and S.C. Solomon, Upper mantle structure beneath the Galapagos Archipelago from surface wave tomography, J. Geophys. Res. (submitted for publication).
[15] M.A. Feighner, M.A. Richards, The fluid dynamics of plume-ridge and plume–plate interactions: an experimental investigation, Earth Planet. Sci. Lett. 129 (1995) 171–182.
[16] G. Ito, J. Lin, C.W. Gable, Interaction of mantle plume and migrating mid-ocean ridges: implications for the Galapagos plume-ridge system, J. Geophys. Res. 102 (1997) 15403–15417.
[17] M.G. Braun, R.A. Sohn, Melt migration in plume-ridge systems, Earth Planet. Sci. Lett. 213 (2003) 417–430.
[18] P.S. Hall, C. Kincaid, Melting, dehydration, and the dynamics of off-axis plume–ridge interaction, Geochem. Geophys. Geosyst. 2 (2003) (paper number 2000GC000137).
[19] M.D. Kurz, D.J. Fornari, J.M. Curtis, M. Perfit, D. Scheirer, D. Geist, The leading age of the Galapagos hotspot: new submarine evidence from Fernandina volcano, Eos, Trans. - Am. Geophys. Union 81 (48) (2000) 1282–1283.
[20] D.S. Wilson, R.N. Hey, History of rift propagation and magnetization intensity for the Cocos–Nazca spreading center, J. Geophys. Res. 100 (1995) 10041–10056.
[21] C.W. Sinton, D.M. Christie, R.A. Duncan, Geochronology of Galapagos seamounts, J. Geophys. Res. 101 (1996) 13689–13700.
[22] U. Barckhausen, C.R. Ranero, R. von Huene, S.C. Cande, H.A. Roeser, Revised tectonic boundaries in the Cocos Plate off Costa Rica: implications for the segmentation of the convergent margin and for plate tectonic models, J. Geophys. Res. 19 (2001) 19207–19220.
[23] T. Simkin, L. Siebert, Volcanoes of the World, Geoscience Press, Tucson, Arizona, 1994.
[24] D.J. Geist, An appraisal of melting processes and the Galapagos hotspot: major and trace-element evidence, J. Volcanol. Geotherm. Res. 52 (1992) 65–82.
[25] M.A. Richard, R.W. Griffiths, Thermal entrainment by deflected mantle plumes, Nature 342 (1989) 900–902.
[26] D. Bercovici, J. Lin, A gravity current model of cooling mantle plume heads with temperature-dependent buoyancy and viscosity, J. Geophys. Res. 101 (1996) 3291–3309.
[27] M.D. Kurz, D. Colodner, T.W. Trull, R.B. Moore, K. O'Brien, Cosmic ray exposure dating with in situ produced cosmogenic 3He: results from young Hawaiian lava flows, Earth Planet. Sci. Lett. 97 (1990) 177–189.
[28] M.D. Kurz, S.K. Rowland, J. Curtice, A.E. Saal and T. Nauman, Eruptions rates at Fernandina volcano, Galapagos Archipelago, from cosmogenic helium, Submitted to Geology, now under review, 2007.
[29] M.D. Kurz, T. Kenna, D. Kammer, J.M. Rhodes, M.O. Garcia, Isotopic Evolution of Mauna Loa Volcano: a View from the Submarine South West Rift, , 1995 289–306 pp.
[30] C.J. Lissenberg, J.H. Bedard, C.R. van Staal, The structure and geochemistry of the gabbro zone of the Annieopsquotch ophiolite, Newfoundland: implications for lower crustal accretion at spreading ridges, Earth Planet. Sci. Lett. 229 (2004) 105–123.
[31] S.R. Hart, J. Blusztajn, H.J.B. Dick, P.S. Meyer, K. Muehlenbachs, The fingerprint of seawater circulation in a 500-meter section of ocean crust gabbros, Geochim. Cosmochim. Acta 63 (23–24) (1999) 4059–4080.
[32] C.J. Garrido, P.B. Kelemen, G. Hirth, Variation of cooling rate with depth in lower crust formed at an oceanic spreading ridge: plagioclase crystal size distributions in gabbros from the Oman ophiolite, Geochem. Geophys. Geosyst. 2 (2001) (Art. No. 2000GC000136).
[33] D.J. Geist, W.M. White, A.R. McBirney, Plume-asthenosphere mixing beneath the Galapagos Archipelago, Nature 333 (657–660) (1988).
[34] D.W. Graham, D.M. Christie, K.S. Harpp, J.E. Lupton, Mantle plume helium in submarine basalts from the Galapagos Platform, Science 262 (1993) 2023–2026.
[35] E.H. Hauri, J.A. Whitehead, S.R. Hart, Fluid dynamic and geochemical aspects of entrainment in mantle plumes, J. Geophys. Res. 99 (1994) 24275–24300.
[36] C. Chauvel, C. Hemond, Melting of a complete section of recycled oceanic crust: trace element and Pb isotopic evidence from Iceland, Geochem. Geophys. Geosyst. 1 (2000) (Paper number 1999GC000002).
[37] A.W. Hofmann, K.P. Jochum, Source characteristics derived from very incompatible trace elements in Mauna Loa and Mauna Kea basalts, Hawaiian Scientific Drilling Project, J. Geophys. Res. 101 (1996) 11831–11839.
[38] A.V. Sobolev, A.W. Hofmann, I.K. Nikogosian, Recycled oceanic crust observed in 'ghost plagioclase' within the source of Mauna Loa lavas, Nature 404 (2000) 986–990.
[39] L.V. Danyushevsky, R.A. Leslie, A.J. Crawford, P. Durancei, Melt inclusions in primitive olivine phenocrysts: the role of localized reaction processes in the origin of anomalous compositions, J. Petrol. 45 (2004) 2531–2553.
[40] H.-J. Yang, F.A. Frey, D. Weiss, A. Giret, D. Pyle, G. Michon, Petrogenesis of the flood basalts forming the northern Kerguelen Archipelago: implications for the Kerguelen plume, J. Petrol. 39 (4) (1998) 711–748.
[41] A.A. Gurenko, A.V. Sobolev, Crust–primitive magma interaction beneath neovolcanic rift zone of Iceland recorded in gabbro xenoliths from Midfell, SW Iceland, Contrib. Mineral. Petrol. 151 (2006) 495–520.
[42] A. Nicolas, A. Prinzhofer, Cumulative or residual origin for the transition zone in ophiolites: structural evidence, J. Petrol. 24 (1983) 188–206.

[43] A. Nicolas, I. Reuber, K. Benn, A new magma chamber model based on structural studies in the Oman ophiolite, Tectonophysics 151 (1988) 87–105.
[44] K. Benn, A. Nicolas, I. Reuber, Mantle–crust transition zone and origin of wehrlitic magmas: evidence from the Oman ophiolite, Tectonophysics 151 (1988) 75–85.
[45] F. Boudier, A. Nicolas, I. Benoît, Magma chambers in the Oman ophiolite: fed from the top and the bottom, Earth Planet. Sci. Lett. 144 (1996) 239–250.
[46] P.B. Kelemen, K. Koga, N. Shimizu, Geochemistry of gabbro sills in the crust–mantle transition zone of the Oman ophiolite: implications for the origin of the oceanic lower crust, Earth Planet. Sci. Lett. 146 (1997) 475–488.
[47] R.A. Dunn, D.R. Toomey, S.C. Solomon, Three-dimensional seismic structure and physical properties of the crust and shallow mantle beneath the East Pacific Rise at 9°30′ N, J. Geophys. Res. 105 (2000) 23,537–23,555.
[48] R.A. Dunn, D.R. Toomey, R.S. Detrick, W.S. Wilcock, Continuous mantle melt supply beneath an overlapping spreading center on the East Pacific Rise, Science 291 (2001) 1955–1958.
[49] R.A. Dunn, D.W. Forsyth, Imaging the transition between the region of mantle melt generation and the crustal magma chamber beneath the southern East Pacific Rise with short-period Love waves, J. Geophys. Res. 108 (B7) (2003), doi:10.1029/2002JB002217 (Article # 2352).
[50] J. Koepke, S.T. Feig, J. Snow, M. Freise, Petrogenesis of oceanic plagiogranites by partial melting of gabbros: an experimental study, Contrib. Mineral. Petrol. 146 (2004) 414–432.
[51] S.R. Hart, Equilibration during mantle melting: a fractal tree model, Proc. Natl. Acad. Sci. 90 (24) (1993) 11914–11918.
[52] Y. Liang, Kinetics of crystal–melt reaction in partially molten silicates. 1. Grain scale processes, Geochem. Geophys. Geosyst. 4 (2003), doi:10.1029/2002GC000375.
[53] J. Crank, The Mathematics of Diffusion, Clarendon Press, Oxford, 1975.
[54] J.-G. Schilling, D. Fontignie, J. Blichert-Toft, R. Kingsley, U. Tomza, Pb–Hf–Nd–Sr isotope variations along the Galapagos Spreading Center (101–83 W): constraints on the dispersal of the Galapagos mantle plume, Geochem. Geophys. Geosyst. 4 (2003), doi:10.1029/ 2002GC000495.
[55] W.F. McDonough, S.-S. Sun, The composition of the Earth, Chem. Geol. 120 (1995) 223–253.